Biochimie 94 (2012) 2559–2568

Contents lists available at SciVerse ScienceDirect

Biochimie

journal homepage: www.elsevier.com/locate/biochi

Research paper

Effects of a halogenated G-quadruplex ligand from the pyridine dicarboxamide series on the terminal sequence of XpYp telomere in HT1080 cells

Assitan Sidibe [a], Florian Hamon [b], Eric Largy [b], Dennis Gomez [c], Marie-Paule Teulade-Fichou [b], Chantal Trentesaux [a], Jean-François Riou [a,*]

[a] Structure des Acides Nucléiques, Télomères et Evolution, Inserm U565, CNRS UMR 7196, Muséum National d'Histoire Naturelle, 43 rue Cuvier, 75231 Paris cedex 05, France
[b] Synthèse et Vectorisation de Biomolécules, CNRS UMR 176, Institut Curie, Bat 110-112, Université Paris-Sud, 91405 Orsay, France
[c] Radiology and DNA repair group, Institut de Pharmacologie et de Biologie Structurale, CNRS UMR 5089, 205 route de Narbonne, 31077 Toulouse, France

ARTICLE INFO

Article history:
Received 29 May 2012
Accepted 5 July 2012
Available online 14 July 2012

Keywords:
G-Quadruplex
Telomere
Pyridine dicarboxamide halogenated derivatives
POT1
C-STELA

ABSTRACT

Non-canonical four-stranded structures called G-quadruplexes can form among telomere repeats during its replication. Small molecule ligands able to interact and to stabilize G-quadruplexes were shown to disrupt the binding of essential telomeric components, such as POT1 and to trigger a telomeric dysfunction associated with a delayed growth arrest in tumor cells. We describe here the chemical synthesis and the G-quadruplex binding properties of three halogenated analogs of the 360A ligand that belongs to the 2,6 pyridine dicarboxamide series. 360A is now commonly used as a benchmark both for biophysical and cellular assays as this compound was shown to display a potent affinity and selectivity for telomeric G-quadruplex DNA over duplex DNA and to induce delayed growth inhibition in HT1080 tumor cell line. Two biophysical assays indicate that, in most cases, the presence of the halogen atom seems to slightly improve the interaction with the telomeric quadruplex. For stability reasons, the bromo derivative (360A–Br) was selected for the cellular assays. Since POT1 participates to the fine tuning of the C-strand end resection during telomere replication, we investigated the effect of 360A–Br to alter the terminal nucleotide composition of XpYp telomere in HT1080 cells using C-STELA. HT1080 cells treated for up to 24 days with 360A–Br presented some minor but significant variations of C-strand terminal nucleotide composition, also observed with a partial siRNA depletion of POT1. The relevance of these minor modifications of the telomeric C-strand resection induced by 360A–Br in HT1080 cells are discussed.

1. Introduction

The nucleoprotein structure at the end of telomeres is essential to maintain chromosome stability and to avoid end of chromosomes to be recognized as a double-strand break by the DNA repair machinery [1]. Human telomeres are composed of tandem repeats of the sequence TTAGGGn and a single-stranded 3′ extension (G-overhang) associated with six proteins from the shelterin complex (TRF1, TRF2, hRAP1, TIN2, TPP1 and POT1) that play important functions in the protection of telomere stability and during its replication [2,3]. Telomeric G-overhang plays a complex role in telomere maintenance. G-overhang provides a template for extension by telomerase or alternative mechanisms of telomere extension based on recombination [4,5]. In addition, G-overhang is essential for the formation of the t-loop, a potential protective structure at telomere, in which the G-overhang invades the telomeric duplex to form a D-loop [6]. Ends of telomeres are generated during replication through a complex mechanism involving G-overhang extension, C-strand resection and C-strand fill-in [7]. Interestingly, the final nucleotide at the 5′ end of the C-strand remains precisely defined, suggesting a fine tuning of the C-strand resection and corresponds to 3′-ATC-5′ (80%) [8]. The nuclease responsible for the C-strand resection is likely to be recruited by the shelterin protein POT1, since the depletion of POT1 by siRNA leads to the randomization of the terminal nucleotide sequence at C-strand [9,10]. The artemis-like nuclease Apollo (hSNM1B) previously found to be associated to the shelterin complex was also found to be implicated in the G-overhang maintenance specifically at telomeres generated by leading strand synthesis and is a potential candidate for the resection enzyme [11].

Evidences are accumulating that non-canonical four-stranded structures called G-quadruplexes can form among telomere repeats

* Corresponding author. Tel.: +33 1 40 79 36 98; fax: +33 1 40 79 37 05.
E-mail address: riou@mnhn.fr (J.-F. Riou).

0300-9084/$ – see front matter © 2012 Elsevier Masson SAS. All rights reserved.
http://dx.doi.org/10.1016/j.biochi.2012.07.003

during lagging strand DNA replication and at the 3′ telomeric G-overhang [12,13]. G-quadruplexes are well characterized conformations of sequences containing several repeats of guanines that arrange in guanine tetrads, stabilized by Hoogsteen hydrogen bounding and coordinated by central cations [12,14]. Human telomeric sequence can form intramolecular G-quadruplexes showing an antiparallel conformation in sodium containing solutions or a parallel "propeller" structure in potassium containing dehydrated solutions or in crystal [15,16]. Although their existence in mammalian cells is based on indirect evidences [13], it has been demonstrated using specific antibodies that G-quadruplexes are formed in the macronuclei from ciliates [17]. Further bioinformatic analysis of the human genome indicated the presence of thousands of potential G-quadruplex-forming sequences (PQS) with a specific enrichment in regulatory regions such as gene promoters, UTRs and splice sequences [18], suggesting a role for G-quadruplexes in the regulation of gene expression.

A large number of small molecule ligands have been synthesized during the last decade to bind and to stabilize G-quadruplexes [19]. Some of them present remarkable selective binding properties to G-quadruplex relative to duplex DNA [20]. G-quadruplex ligands were shown to induce a delayed growth arrest or apoptosis in both telomerase positive and ALT tumor cell lines associated with alterations of the telomere stability [12,19,21]. All G-quadruplex ligands were shown to interfere more or less with the binding of essential shelterin components, such as POT1 and TRF2, leading to a DNA damage response at telomere (TIFs) and G-overhang shortening [22–32].

G-quadruplex ligands also induce telomere-independent DNA damage foci or binding sites that might be related to the presence of G-quadruplexes in other regions of the genome [25,33], as evidenced recently for pyridostatin [34]. These effects correspond to the lack of selectivity reported for all G-quadruplex ligands between telomeric over the others G-quadruplexes [35,36] that may be explained by their predominant binding mode through aromatic π stacking to one of the external G4 quartet [16]. In some cases, minor chemical modifications of G4-ligands were reported to affect both their biophysical and biological properties. As an example, compare ligands 360A, 307A and 832A from the 2,6 pyridine dicarboxamide series for G4-FID displacement assay and growth inhibition in tumor cell lines in [31,36]. Indeed, compounds presenting a close G-quadruplex binding profile (360A and Phen-DC3) displayed remarkable differences at the level of transcriptional changes in quadruplex-containing genes [36,37]. Altogether these observations suggest that minor modifications of the G-quadruplex ligand structure and of the G-quadruplex binding profile might have an important impact on their overall biological activity.

In this study, we have investigated the impact of the introduction of a halogen atom (Cl, Br, I) on the central pyridine moiety. The introduction of halogen atoms on biologically active compound is classically used in drug design and is known to improve membrane permeability (cellular and blood brain barrier). In addition steric and electronic effects of halogen atoms may improve binding to molecular targets [38]. Thus both improvements of 360A activity could be expected both in terms of quadruplex recognition and in terms of cellular effects.

The three chloro, bromo and iodo derivatives (360A–Cl, 360A–Br, 360A–I) were evaluated for their quadruplex interaction *in vitro* using biophysical and biochemical assays. In addition, because all G-quadruplex ligands were reported to alter the binding of POT1 at telomere and that this shelterin protein controlled the C-strand resection processes, we have also studied the alterations of the C-strand nucleotide composition at XpYp telomere in HT1080 cells using C-STELA with the bromo derivative (360A–Br). We report that 360A–Br retains the potent affinity and selectivity for telomeric G-quadruplex and delayed growth inhibitory properties, but triggers mild modifications of the telomeric C-strand in agreement with a partial displacement of POT1, whose significance is discussed.

2. Materials and methods

2.1. Synthesis

1H and 13C spectra were recorded at 25 °C on a Bruker Avance 300 using TMS as internal standard. Deuterated $CDCl_3$ and DMSO-d_6 were purchased from SDS. The following abbreviations are used: singlet (s), doublet (d), triplet (t) and multiplet (m). Low resolution mass spectrometry (ESI-MS) was recorded on a micromass ZQ 2000 (waters). High resolution mass spectrometry (ESI-MS) were provided by the I.C.S.N. (Institut de Chimie des Substances Naturelles, Gif-sur-Yvette). TLC analysis was carried out on silica gel (Merck 60F-254) with visualization at 254 and 366 nm. Melting points were taken on a Kofler melting point apparatus and are uncorrected. Preparative flash chromatography was carried out with Merck silica gel (Si 60, 40–63 μm). Reagents and chemicals were purchased from Sigma-aldrich, Acros or Alfa-aesar unless otherwise stated. Solvents were purchased from SDS.

2.2. FRET experiments

Quantitative FRET experiments were obtained on a Stratagene MX3000P (La Jolla, CA) quantitative PCR apparatus using 0.2 μM F21T (5′-FAM-GGGTTAGGGTTAGGGTTAGGG-Tamra-3′). Melting profiles were recorded in a 10 mM lithium cacodylate (pH 7.2) buffer with 100 mM NaCl or 10 mM KCl + 90 mM LiCl. Excitation wavelength was 496 nm and emission was recorded at 516 nm. For competition experiments, various concentrations of the double-stranded ds26 competitor (5′-CAATCGGATCGAATTCGATCCGATTG-3′) were added prior to the melting experiment.

2.3. HT-G4-FID

HT-G4-FID measurements were performed as described previously [39], on a FLUOstar Omega microplate reader (BMG Labtech) with a 96-well black quartz microplate (Hellma). TO (thiazole orange) and cacodylic acid were purchased from Aldrich and used without further purification. Stock solutions of TO and ligands (2 mM in DMSO) were used. 22AG oligonucleotide (corresponding to the human telomeric repeat; [5′-$AG_3(T_2AG_3)_3$-3′]), purified by reverse phase HPLC, was purchased from Eurogentec (Belgium).

The percentage of displacement is calculated from the fluorescence intensity (F), using: TOD (%) = $100 - [(F/F_0) \times 100]$, F_0 being the fluorescence from the fluorescent probe bound to DNA without added ligand. The TOD is then plotted as a function of the concentration of added ligand. The ligand affinity was evaluated by the concentration of ligand required to decrease the fluorescence of the probe by 50%, noted DC_{50}, and determined after non-linear fitting of the displacement curve.

2.4. EMSA experiments

Topo IIIα was purified according to a previously published procedure [40]. Electrophoretic mobility shift assays using Topo III was performed in 10 μL of the following solution: 50 mM HEPES (pH 7.9), 100 mM NaCl, 0.1 mM EDTA, 4% w/v sucrose, 2% v/v glycerol, 0.1 mg/mL BSA, 0.02% w/v bromophenol blue, 20 nM labeled 22AG (5′-AGGGTTAGGGTTAGGGTTAGGG-3′) and Topo III (100 nM). The indicated concentrations of ligands were added in a volume of 1 μL. The reaction mixture was incubated at room

temperature for 30 min. Each individual mixture was separated immediately by electrophoresis on 1% agarose gels in 0.5× Tris-Borate-EDTA buffer. The gels were run at 80 V for 45 min, dried on Whatman DE81 paper, and visualized by a phosporimager (Typhoon 9210, Amersham). Data was analyzed using ImageQuant software (Amersham) and results were expressed relative to the fraction of DNA bound to Topo III in the absence of treatment, defined as 100%. Values correspond to the mean value of three independent experiments ± SD.

2.5. Cell culture and drug treatment

Human HT1080 fibrosarcoma cell line was obtained from the American Type Culture Collection (Rockville, MD). Cells were cultured in DMEM with glutamax, supplemented with 10% fetal calf serum at 37 °C in an atmosphere containing 5% CO2. For growth inhibition experiments, HT1080 cells were seeded at 50,000/mL in 75 cm^2 culture dish and after 72 h of treatment, cells were trypsinised, counted and results expressed relative to cells treated with DMSO, defined as 100%, represent the mean value of two independent experiments. Other cell lines, KB, A549, MCF7, HCT116 and MRC5, were assayed for growth inhibition at 1 and 10 μM for 72 h in the cellular platform from the Institut de Chimie des Substance Naturelles (CNRS UPR 2301, Gif-sur-Yvette, France), each point in triplicate. For cell senescence experiments, HT1080 cells were seeded at 40,000/mL in 75 cm^2 culture dish. After 4 days of treatment, cells were trypsined, counted and replated at 40,000/mL. At each passage, population doubling (PD) from untreated or ligand-treated cultures were calculated according to the formula: PD = Log Cell density Day 4 − Log 40000/Log 2.

2.6. Single telomere length analysis

The C-STELA assay was performed as described previously [8,41]. Each DNA sample was prepared in parallel from HT1080 treated or untreated cells using QIAamp DNA mini kit (Qiagen) and ligation reactions were perfomed with individual C-telorettes:

C-telorette 1: 5′-TGCTCCGTGCATCTGGCATCCCCTAAC-3′;
C-telorette 2: 5′-TGCTCCGTGCATCTGGCATCTAACCCT-3′;
C-telorette 3: 5′-TGCTCCGTGCATCTGGCATCCCTAACC-3′;
C-telorette 4: 5′-TGCTCCGTGCATCTGGCATCCTAACCC-3′;
C-telorette 5: 5′-TGCTCCGTGCATCTGGCATCAACCCTA-3′;
C-telorette 6: 5′-TGCTCCGTGCATCTGGCATCACCCTAA-3′.

For each ligation, EcoR1 digested DNA (80 ng) was incubated overnight at 37 °C in 20 μL of reaction mix (1× ligase buffer, 10 U of T4 ligase and 10^{-3} μM of each C-telorette). PCR amplification reactions were performed with 2 ng of ligated DNA, 1 μM primers [XpYpE2 (forward primer subtelomeric): 5′-TTGTCTCAGGGTCCTAGTG-3′; C-teltail (reverse primer): 5′-TGCTCCGTGCATCTGGCATC-3′], 1U of Failsafe enzyme mix in 1× Failsafe buffer H (Epicenter) in a final volume of 25 μL for 26 cycles of 95 °C for 15 s, 58 °C for 20 s, and 72 °C for 10 min.

Amplification products were resolved on a 0.8% agarose gel, denatured, transferred onto a positively charged nylon membrane (Hybond N+), fixed with UV, and hybridized with the telomeric probe 24CA end-labeled with γ[^{32}P]-ATP with T4 kinase. Telomeric fragments were exposed on a screen and revealed with a phosporimager (Typhoon 9210, Amersham). Data were analyzed using ImageQuant software (Amersham) for radioactivity on the whole lane or for the number of telomere (as indicated in the text) on at least three independent ligations and statistical analysis was performed using student test.

2.7. SiRNA experiments

For siRNA experiments, HT1080 cells were plated in 6-well culture plates at 1 × 10^5 cells/well in 2 mL DMEM medium without antibiotics. After 12 h, 100 nM siRNA POT1ex7 were transfected for 4 h, using Lipofectamin 2000 (Invitrogen). A second transfection was performed 24 h later with 100 nM siRNA POT1ex18. 2 days after the last transfection, treated cells were processed for Western-blotting with POT1 antibody or for C-STELA experiments. The siRNA used here are:

siRNA POT1ex7: 5′-GGGUGGUACAAUUGUCAAU-3′,
siRNA POT1ex18: 5′-GUACUAGAAGCCUAUCTCA-3′,
siRNA control: 5′-UGCGCUACGAUGGACGAUG-3′.

2.8. Antibodies and western blot analysis

Cells were washed with ice-cold PBS and lysed in buffer (Tris–HCl pH 7.4 50 mM, NP40 1%, NaCl 150 mM, EDTA 1 mM, PMSF 1 mM) including a protease inhibitor cocktail at 1 μg/mL (Mini complete protease, Roche Diagnostics). After 30 min on ice, lysates were cleared by centrifugation. Protein concentration was quantified with the Bio-Rad protein assay. Cell lysates containing equal amounts of total protein (25 μg) were resolved on a 10% SDS-

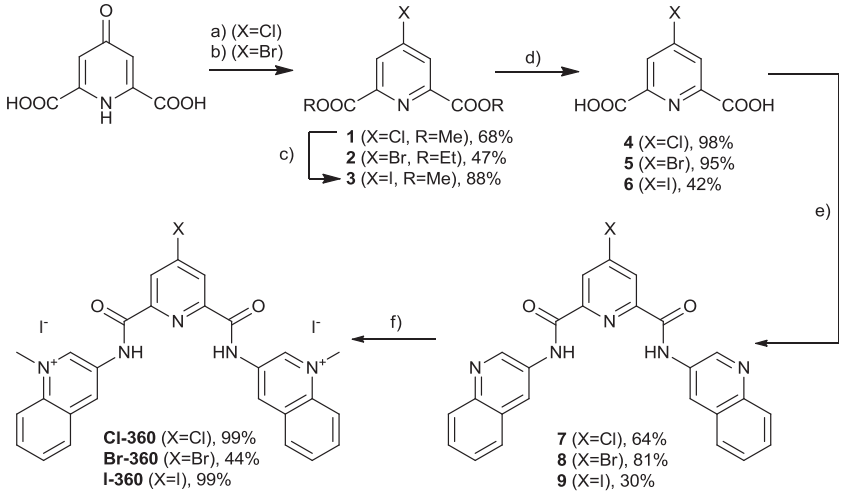

Fig. 1. Chemical synthesis of halogenated 360A derivatives (360A–X). Synthesis: a) 1) Ph-$POCl_2$, 120 °C, 2 h, 2) MeOH, 0 °C, 1 h; b) 1) PBr_5, 90 °C, 6 h; 2) absolute EtOH, 0 °C; c) aq. LiOH, THF, 3 h, RT or aq. NaOH, reflux, 1 h then HCl; d) 3-aminoquinoline, EDCi, HOBt, DMF (CH_2Cl_2), 16 h, RT; e) CH_3I, DMF (MeOH), 50 °C, see also Supplementary information for more detailed procedures.

polyacrylamide gel by electrophoresis, transferred to PVDF-membrane (Macherey-Nalgel) by electro-blotting in 25 mM Tris–HCl pH 8.3, 192 mM glycine, 20% ethanol. Membranes were blocked for 3 h at room temperature in 10 mM Tris–HCl pH 7.5 containing 0.15 M NaCl, 0.1% Tween 20 and 5% nonfat dry milk. Primary and secondary immunodetection, as well as washes, were performed in the same buffer using 5% dry milk. Western blot analysis was accomplished according to standard procedure using SuperSignal West Pico chemiluminescent substrate (Pierce). The following primary antibodies were used: Monoclonal anti-β actin clone AC-15 (Sigma) (1:5000), anti-cleaved PARP asp 214 (Cell signaling) (1:1000), anti P21 (BD Pharmingen) (1:1000), anti POT1 #21382 (Abcam) (1:1000).

3. Results

3.1. Synthesis of the three halogenated 360A derivatives

Halogenated **360A** derivatives (**360A**–**X**) were prepared following a common synthetic pathway (Fig. 1). First, chloration of chelidamic acid was carried out in phenylphosphonic dichloride followed by methanolysis at 0 °C affording the corresponding dimethyl ester **1** with a 68% yield over the two steps. The corresponding iodo compound **3** was obtained by halogen–halogen exchange (Finkelstein reaction, 88% yield) [42]. Similarly, bromination of chelidamic acid in phosphorus pentabromide was carried out followed by ethanolysis at 0 °C leading to diester **2** with 47% yield over the 2 steps. Hydrolysis of three halogeno-derivatives was conducted either with LiOH in aqueous THF or with an aqueous solution of NaOH with yield ranging from 42% to 98%. The corresponding diacids **4**, **5** and **6** were then coupled to 3-aminoquinoline in presence of EDCI and HOBt in DMF with yield comprised between 30 and 81%. Finally methylation of **7**, **8** and **9** by iodomethane in a solvent mixture afforded 360A–Cl, 360A–Br and 360A–I with 99%, 44% and 99% yield respectively. The overall yields for the synthesis of the three **360A**–**X** compounds are 42, 16% and 7% over 5, 5 and 6 steps, respectively.

3.2. FRET, HT-G4-FID and EMSA analysis

The ability of 360A-halogenated derivatives to stabilize the telomeric G-quadruplex DNA (F21T) was evaluated in a FRET-melting temperature assay, in comparison with **360A**. Melting temperature shifts were compared at a drug concentration of 1 μM and using 0.2 μM F21T and the experiment was conducted both in Na^+ and K^+ rich buffer, results are summarized in Fig. 2A. All compounds show very high affinity for the human telomeric G-quadruplex sequence F21T, leading to increases in melting temperature ($\Delta T_{1/2}$) of 23–27 °C in Na^+ (NaCl 100 mM) and of up to 25–28 °C in K^+ (KCl 10 mM, LiCl 90 mM). The chloro derivative **360A**–**Cl** represents the exception with a strikingly low binding in K^+ conditions whereas it is strongly active in Na^+ conditions (Fig. 2A). The selectivity of the ligands for the G-quadruplex structure subsequently was evaluated in a competitive FRET-melting experiment, in which different amounts (3 and 10 μM) of duplex DNA (ds26) were added to the telomeric sequence F21T (0.2 μM). In the presence of 10 μM of ds26 competitor (*i.e.*, a 50-fold molar excess *vs* F21T), the strong stabilization induced by both ligands was not significantly lowered (from 0 to 2 °C), thereby suggesting a high affinity and selectivity for telomeric G-quadruplex over duplex DNA, as previously reported for this series [31,36]. Finally, the high binding affinity of the three halogeno compounds was confirmed using the HT-G4-FID assay (Fluorescent Intercalator Displacement assay) (Fig. 2B). DC_{50} values (concentration of ligand displacing 50% of the fluorophore) similar to that of **360A** (around 0.40–0.45 μM) were found for the bromo and iodo compounds independently of the cation present in the medium. In consistency with the FRET data, the chloro compound was found significantly less active in K^+ as compared to the two other derivatives. However the same is observed in Na^+ which was not the case in the FRET-melting experiment. Altogether the low DC_{50} obtained sorts the bromo and iodo compounds among the most potent G4-ligands evaluated so far in this assay [39]. Altogether the data collected from the two assays indicate that the sterically demanding bromo and iodo substituents have no negative influence on the binding strength of the quadruplex/ligand interaction. On the opposite, the introduction of halogen atom seems to afford a slight advantage considering that all $\Delta T_{1/2}$ values are higher and most DC_{50} values are lower thereby suggesting a stronger association to G-quadruplex as compared to that of **360A** (Fig. 2A).

The different behavior of the chloro derivative is difficult to rationalize on the ground of electronegativity and steric considerations, this will be studied further in the light of recently identified halogen bonds in drug–target complexes [38]. For this reason and owing to the poor metabolic stability of iodo compounds only the bromo derivative was used for the biochemical and cellular assays.

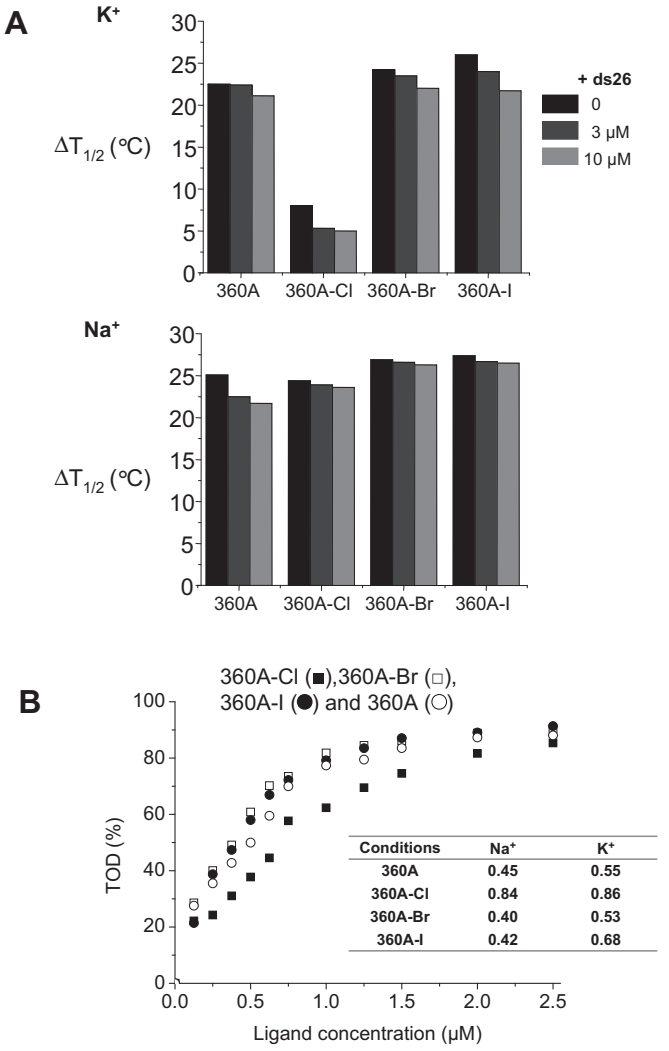

Fig. 2. FRET melting and G4-FID assays of halogenated 360A derivatives. (A) F21T (0.2 μM) FRET-based $\Delta T_{1/2}$ values (°C) for 360A, 360A–Cl, 360A–I and 360A–Br (1 μM) at the indicated ionic conditions (K^+ or Na^+) in the presence or absence of ds26 competitor. (B) HT-G4-FID assay using the human telomeric sequence 22AG with different concentrations of 360A derivatives, as indicated. Results are expressed in percent of TO Displacement (TOD; %). DC_{50} values (μM) for K^+ or Na^+ conditions are indicated in the table.

The inhibition of Topo IIIα binding to a telomeric DNA sequence 22AG by the ligands **360A** and **360A**–**Br** were examined *in vitro* using EMSA assays [43]. Both compounds inhibit the binding of Topo IIIα at low micromolar concentrations (Fig. 3), with IC_{50}'s equal to 1.2 and 0.7 μM for **360A** and **360A**–**Br**, respectively. This result suits well with the G-quadruplex stabilizing properties of these ligands, by analogy with other compounds previously examined in this assay [43,44]. All together, the FRET and EMSA *in vitro* results suggest that **360A**–**Br** derivative presents a slightly higher interaction with telomeric G-quadruplex as compared to the benchmark compound **360A** and retains the exceptionally high selectivity of the latter toward duplex DNA.

3.3. Growth inhibitory properties on cell lines

Pyridine dicarboxamide derivative **360A** was reported to induce a delayed growth inhibition in different tumor cell line models, associated with the induction of telomeric instability, as shown by telomere-end fusion and G-overhang shortening [31,45]. To determine whether the substitution with a bromine influences cellular growth inhibitory properties of the series, short-term antiproliferative effect (72 h) was examined against different cell lines, using 10 μM of compound (Fig. 4). Results indicated that **360A** and **360A**–**Br** were inactive against the normal cell line MRC5 and presented weak growth inhibitory properties (ranging from 5 to 25%) against KB, A549, MCF7 and HCT116 tumor cell lines, as expected for a specific G-quadruplex ligand. Interestingly, HT1080 tumor cell line was found to be more sensitive to **360A**–**Br** than **360A.** These data suggested that the introduction of the Bromine moiety at position 4 of the pyridine has at least a neutral or a slight advantage to improve the cellular activity.

In order to examine the long-term effects of **360**–**Br**, HT1080 and A549 cells were treated with 10 μM of ligand for 24 and 21 days, respectively. Treated cells were replated every 3 or 4 days (with fresh compound added at each replating) and the cumulated population doubling was measured (Fig. 5A). Results show that **360A**–**Br** induced a decrease of the population doubling starting between days 4 and 8 on both cell lines and corresponding to a delayed growth inhibition. After 24 or 21 days of treatment, the population doubling in HT1080 and A549 cells was reduced to 42% and 37% of controls, respectively. Western blot experiments, using cleaved-PARP and P21 antibodies, were performed on A549 cells during the time-course of **360A**–**Br** treatment. Results presented in Fig. 5B indicated that **360A**–**Br** induces a significant increase of P21 expression but does not trigger any expression of cleaved-PARP, as compared to camptothecin treatment (0.5 μM for 24 h). Thus, these results are in agreement with a delayed growth inhibition associated with the activation of P21, a figure already reported for different G-quadruplex ligands [32,46,47].

3.4. Effect of 360A–Br on the C-strand terminal nucleotide composition of XpYp telomere

G-quadruplex ligands, such as telomestatin, RHPS4, pyridostatin and BRACO-19 have been reported to trigger POT1 removal from telomeres [22,26–28,30]. Interestingly, depletion of POT1 by shRNA

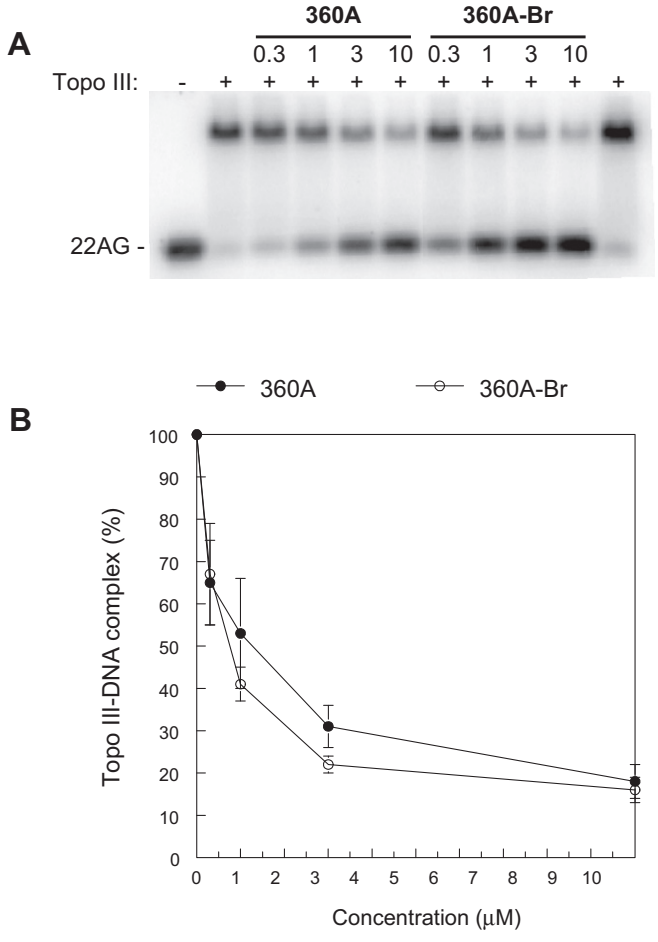

Fig. 3. Inhibition of Topo III binding to the telomeric sequence 22AG by 360A and 360A–Br. (A) Representative bandshift assay using purified Topo III (100 nM) and [32]P-labeled 22AG (20 nM) in the presence of the indicated concentrations (μM) of 360A or 360A–Br on the top of the panel. Control 22AG alone is indicated by (–). (B) Quantification of the bandshift experiments with 360A (closed circles) or 360A–Br (open circles). Results correspond to the mean ± SD of three determinations and were expressed relative to the fraction of Topo III bound to 22AG, defined as 100%.

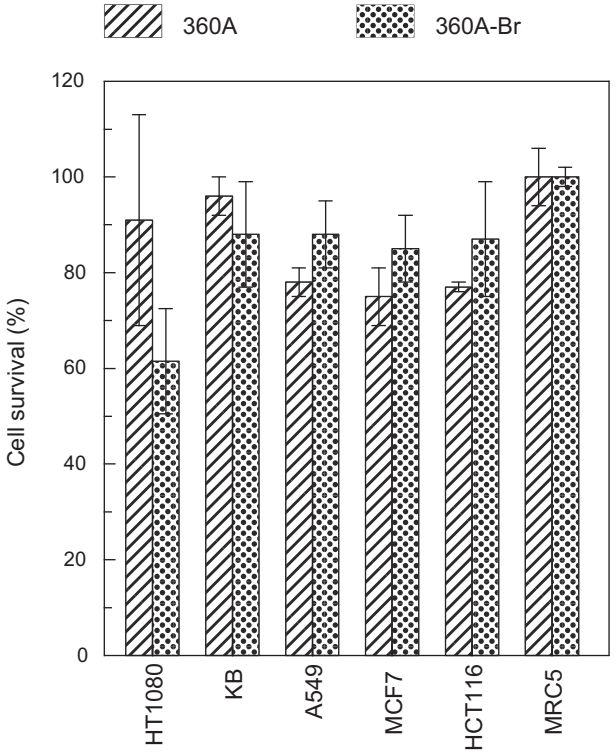

Fig. 4. Antiproliferative activities of 360A and 360A–Br against a panel of human cell lines. Cells were treated with 10 μM of compounds for 72 h and results (mean ± S.E.) expressed in percent of untreated controls, defined as 100%.

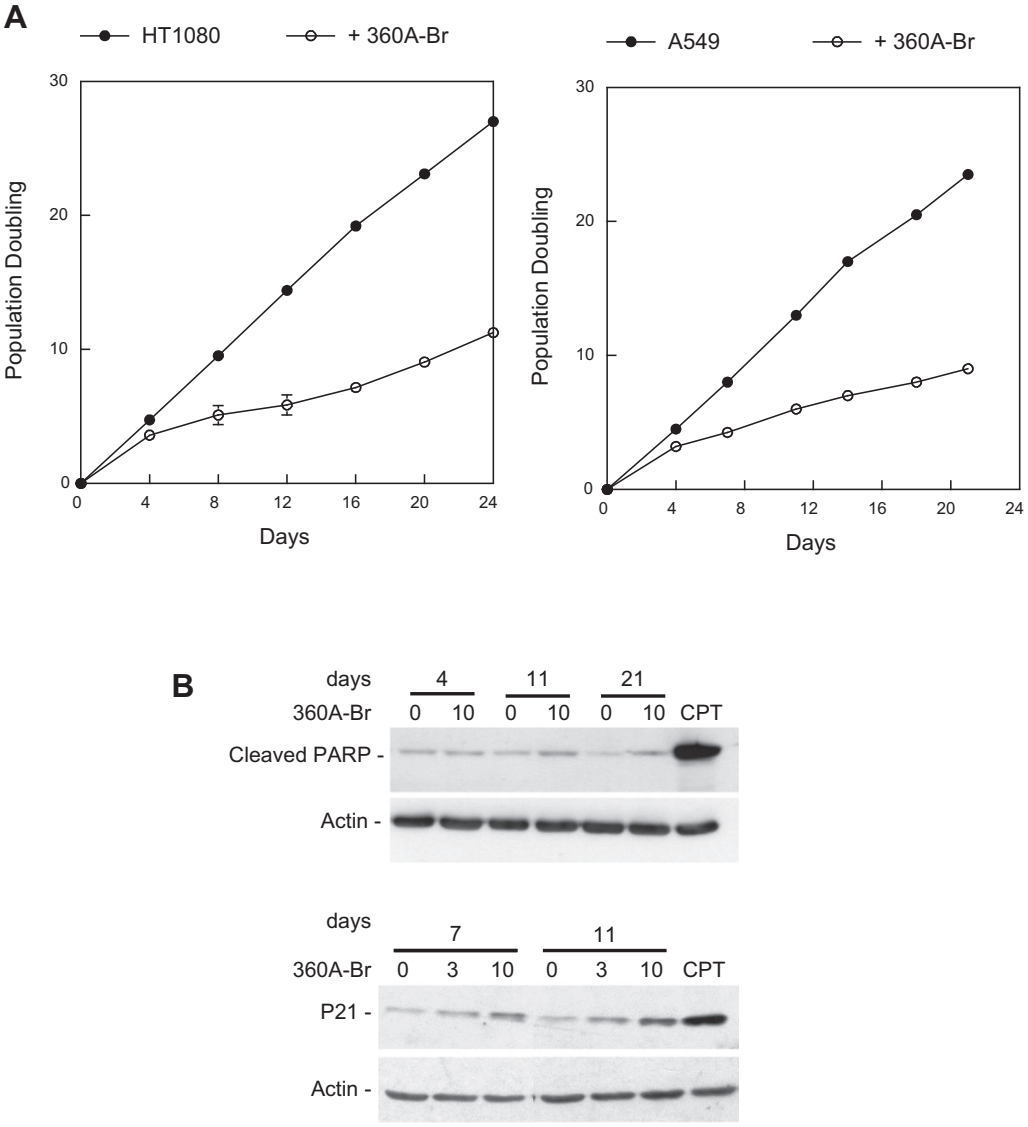

Fig. 5. 360A–Br induced a delayed growth inhibition in human tumor cell lines without apoptosis. (A) Long-term proliferation inhibition of A549 and HT1080 cells induced by 360A–Br (10 μM). Cells were treated for the indicated times (21 or 24 days) and results represent the cumulated population doubling measured at each replating in control untreated cells or 360A–Br-treated cells. (B) Western blot analysis of cleaved-PARP and P21 protein expression in A549 cells untreated or treated with 360A–Br (3 or 10 μM) for the indicated times (3, 11 or 21 days). Camptothecin (CPT, 0.5 μM for 24 h) was used as a positive control for cleaved-PARP and P21 expression. β-actin was used as a control for protein loading.

or siRNA was found to alter the C-strand resection leading to the randomization of the terminal telomeric sequence [9,10]. To address whether cell treatment by 360A–Br induces a modification of the terminal nucleotide composition, we have investigated by C-STELA analysis the composition of the terminal nucleotide at the C-strand of XpYp telomere during the long-term treatment of HT1080 cells. In this assay, C-telorettes #1 to #6, representing the six possible ends of the 5′ C-strand telomeric sequence were individually ligated to DNA samples extracted from HT1080-treated cells, using the telomeric overhang as a template for annealing [8]. Each ligation product is amplified with a sequence (C-teltail) common to all C-telorettes and a primer that anneal to a XpYp subtelomeric site present at 450 bases from the start of the telomere repeats [41,48]. Individual telomeres, corresponding to discrete bands are revealed by southern blot hybridization and are proportional to the number of ligated telomeres. In our hands, the C-STELA assay showed the expected predominance of the ATC-5′ in untreated HT1080 cells since C-telorette #3 corresponded to 64% of the ligated and amplified telomeres (Fig. 6). We also found, that C-telorettes #2 and #4 corresponding to CAA-5′ and AAT-5′ ends, and immediately adjacent to ATC-5′, are ligated with a non-negligible percentage, equal to 20 and 12.5%, respectively.

C-STELA analysis of HT1080 cells treated by **360A–Br** was performed on DNA samples harvested at each passages (days 4, 8, 12, 16, 20 and 24 days) and representative gels of the C-telorette profile indicated that the overall ATC-5′ predominance is conserved under drug treatment, as compared to untreated HT1080 cells (Fig. 7A). Quantification of the experiments only revealed a non-significant change of the C-telorette ligation profile, when all treated DNA samples (day 4 to day 24) were compared to the overall untreated controls (Fig. 7B). However, a significant decrease to 8.5% ($p < 0.005$) and increase to 20.4% ($p < 0.05$) in the proportion of the ligation of C-telorette #2 and #4 corresponding to the CAA-5′ and AAT-5′ telomere ends, respectively were found during the first part of the cell treatment (days 4–12) (Fig. 7C, see also Fig. S1) where the growth inhibition is the most pronounced (compare days 4–12 and

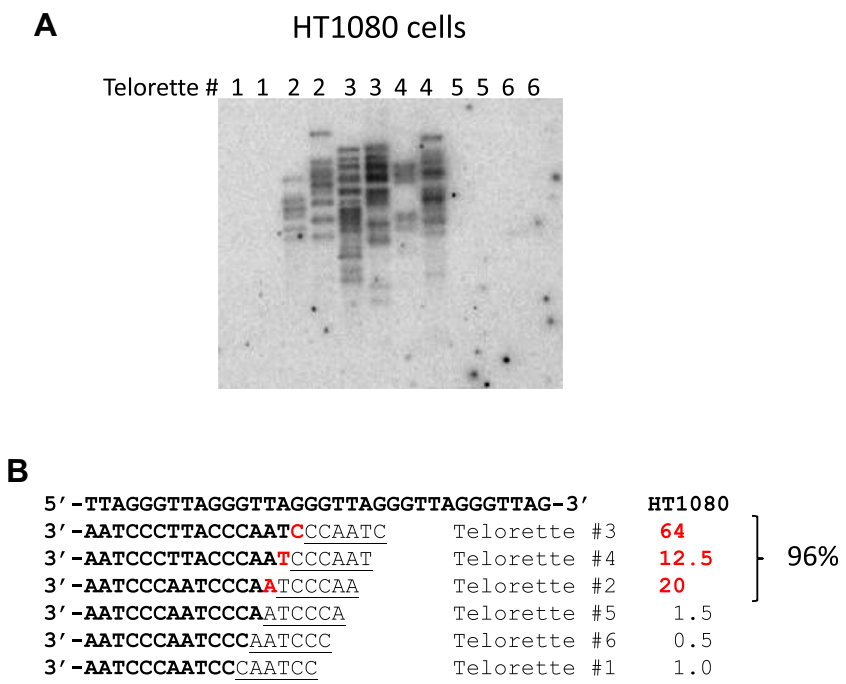

Fig. 6. Terminal nucleotide composition at telomeric C-strand in HT1080 cells. (A) Individual telomere products generated by the C-STELA assay in HT1080 cells (see Materials and methods). Each C-telorette was used in an independent assay (duplicate ligation in this example) and run in independent lanes. C-telorette number (#1–6) is indicated at the top of the gel. The hybridizing part of the telorette is underlined. (B) Schematic representation of XpYp telomere 3′ G-overhang and 5′ C-strand, with the terminal nucleotide composition corresponding to each individual C-telorette at C-strand. The relative percentage (mean) generated by each individual C-telorette is indicated on the right of the panel and corresponds to the quantification of 15 independent ligation assays. The total telomere signal generated by the six C-telorettes in each assay and quantified by ImageQuant (on the whole lane) is defined as 100%. See also Fig. 7, for the S.D. values of the assay. Individual telomeres generated by C-telorettes #2, 3 and 4 contributed to 96% of the total signal in untreated HT1080 cells.

16–24 in Fig. 5A). In contrast, during the second part of the treatment (days 16–24), the C-telorette ligation profile becomes again similar in proportions to untreated controls. It must be noticed that a reproducible decrease of the efficiency of telomere ligation and/or PCR amplification reaction was also observed during this stage (see days 16–24 in Fig. 7B). Indeed, the mean telomere number in untreated and treated cells (days 20–24) is equal to 38.8 and 23.3 ($p < 0.05$), respectively (Fig. 7D). Such effect was also found after long-term treatment of HT1080 cells with another PDC derivative (360A-biot) [49](A. Sidibe, data not shown) and may be due to the accumulation of DNA lesions occurring at telomere, such as telomere-end fusions, telomere doublets or deletions that were detected by this class of ligand (360A) in different tumor cell lines [45,50].

In order to determine the sensitivity of the C-STELA assay to detect the randomization of the telomeric C-strand, we have also evaluated the effect of POT1 depletion using siRNA directed against POT1. HT1080 cells were transfected with siRNA control or with two different siRNA directed against POT1 that were previously reported [10]. Western blot experiments indicated that siRNA directed against exon 18 of POT1 gene (siPOT1ex18) induced a significant decrease of POT1 (50%), but not siRNA directed against exon 7 (siPOT1ex7) in HT1080 cells, 72 h after transfection (Fig. 8A). In parallel, C-STELA analysis of HT1080 cells depleted for POT1 protein by siRNA POT1ex18 was performed and compared to HT1080 cells treated with siRNA control (Fig. 8B). Results from triplicate ligations on HT1080 treated with siRNA control showed a more marked ATC-5′ predominance in this experiment since products from telorette #3 corresponded to 83% and the absence of products from telorette #4 (Fig. 8B and C). We attribute these variations to differences in the quality of the DNA preparations and/or efficiency in the ligation reaction (see Discussion). After treatment with siRNA POT1ex18, a partial randomization of the terminal nucleotide sequence was observed, as revealed by a decrease of the products from telorettes #2 and 3 and the increase of those from telorettes #4 and 6, suggesting that the partial loss of POT1 is sufficient to trigger a detectable alteration of the C-telorette ligation profile.

Interestingly, we observe a similar alteration of C-telorette profile between **360A–Br** treatment (days 4–12) and POT1 depletion (compare the relative decrease of C-telorette #2 and the relative increase of C-telorette #4 in Figs. 7C and 8C), suggesting that in our experimental conditions the effect of the ligand may correspond to a partial depletion of POT1.

4. Discussion

The **360A–Br** PDC derivative reported in this paper shows high affinity for telomeric G-quadruplex DNA, as evidenced by different techniques such as FRET-melting, G4-FID and EMSA assays and retains the high selectivity toward duplex DNA of 360A. In agreement, the substitution at position 4 of the pyridine by a 2-aminoethoxy (pyridostatin) or by a biotin (PDC-biotin) were also shown to maintain the affinity and the selectivity toward telomeric G-quadruplex in this series [34,49].

Although the panel of cell line used here is limited, our results indicated that **360A** and **360A–Br** could not be discriminated through their cellular activity at short-term (72 h). Both compounds were found inactive against the normal cell line MRC5, suggesting an *in vitro* selective activity for tumor cells as already reported for other selective G-quadruplex ligands such as telomestatin [51], 307A [31] and pyridostatin [52].

In contrast to its close analog 307A in glioma cells lines [31] or to the triazine derivative 12459 in A549 cells [47], we do not observe any apoptotic process induced by 360A–Br in A549 or HT1080 cells, but rather a delayed growth inhibition associated with the activation of P21. Interestingly, pyridostatin and different analogs also

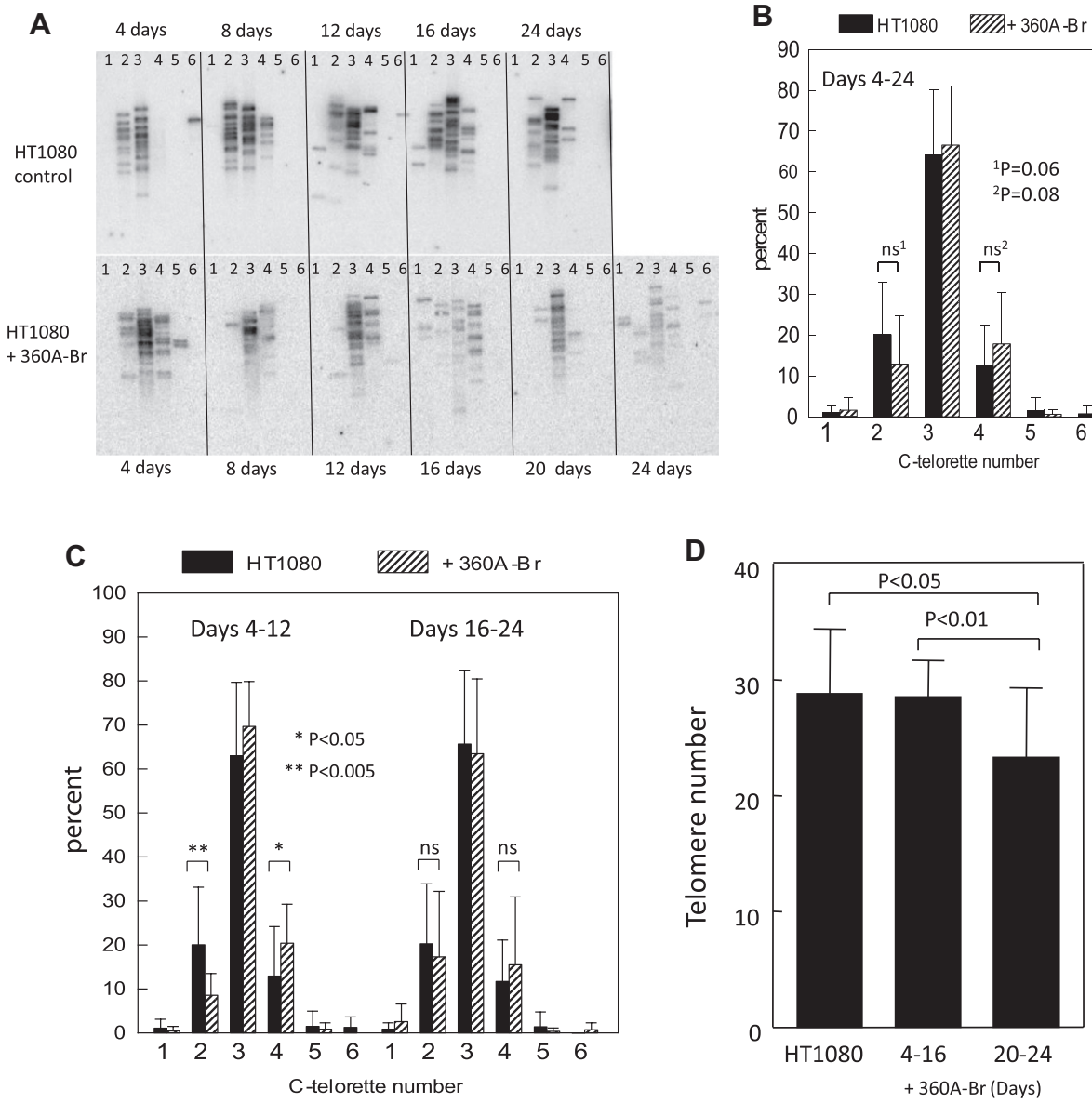

Fig. 7. Effect of 360A–Br on the terminal nucleotide composition at telomeric C-strand in HT1080 cells. (A) Representative experiments of the C-STELA assay from HT1080 cells untreated or treated with 360A–Br (10 μM) harvested at the indicated days. C-telorette number (1–6) is indicated. (B) Quantification of the relative percentage (mean ± SD) generated by each individual C-telorettes in HT1080 cells untreated or treated by 360A–Br. In each lane, the telomere signal generated was quantified and expressed in percentage, the total telomere signal generated by the six telorettes in each ligation defined as 100%. Untreated controls corresponded to 15 independent ligations and treated to 18 independent ligations. *P* values after statistical analysis by student test are indicated. (C) Same analysis that differentiates days 4–12 and 16–24 of the treatment by 360A–Br, as indicated. Ns corresponded to $p > 0.05$. (D) Total telomere number generated by the six C-telorettes in each ligation. Results corresponded to the mean ± SD for untreated HT1080 (HT1080, $n = 15$), HT1080 treated with 360A–Br (days 4–16, $n = 12$ and days 20–24, $n = 6$).

induced a senescence-like phenotype in HT1080 cells during long-term treatments but did not induce an elevated level of cell death [52]. Both pyridostatin and 360A trigger a partial delocalization of POT1 from telomeres in this cell line ([26] and result not shown). This suggests a common phenotypic action of PDC ligands in HT1080 cells.

Thus, we used **360A–Br**, as a representative member of the PDC series, to further investigate its effect to randomize the telomeric C-strand by using the C-STELA assay in HT1080 cells. Since depletion of POT1 by shRNA was shown to alter the C-strand resection, leading to the randomization of the C-strand, we expected to obtain an easily detectable effect on C-STELA, after **360A–Br** treatment.

We first noticed some variations in the C-STELA assay profile in HT1080 cells, compared to the original report on BJ cells [8], and concerning the presence of a significant amount of AAT-5′ and CAA-5′ ends in untreated HT1080 cells. These variations were also observed for other cells lines in this report and in ulterior studies [8–10]. Comparison between different cell lines confirmed the predominance of ATC-5′, but in proportion varying from 35 to 50% (see Fig. S1 in [8]) or equal to 100% [10]. In these studies, AAT-5′ ends were found present, varying from 10 to 20%, in agreement with our finding. It is possible that these differences result from minor differences in the experimental protocol for C-STELA (see Table S1), or from the used cell line. However, we also observed a variation between two series of experiments using HT1080 cells concerning the detection of AAT-5′ ends (compare telorette #4 in Figs. 7 and 8). Since these DNA samples were prepared at different dates, these variations may be due to differences in the quality of the DNA preparation and/or efficiency in the ligation reaction. In order to limit these reproducibility issues, DNA extraction for all

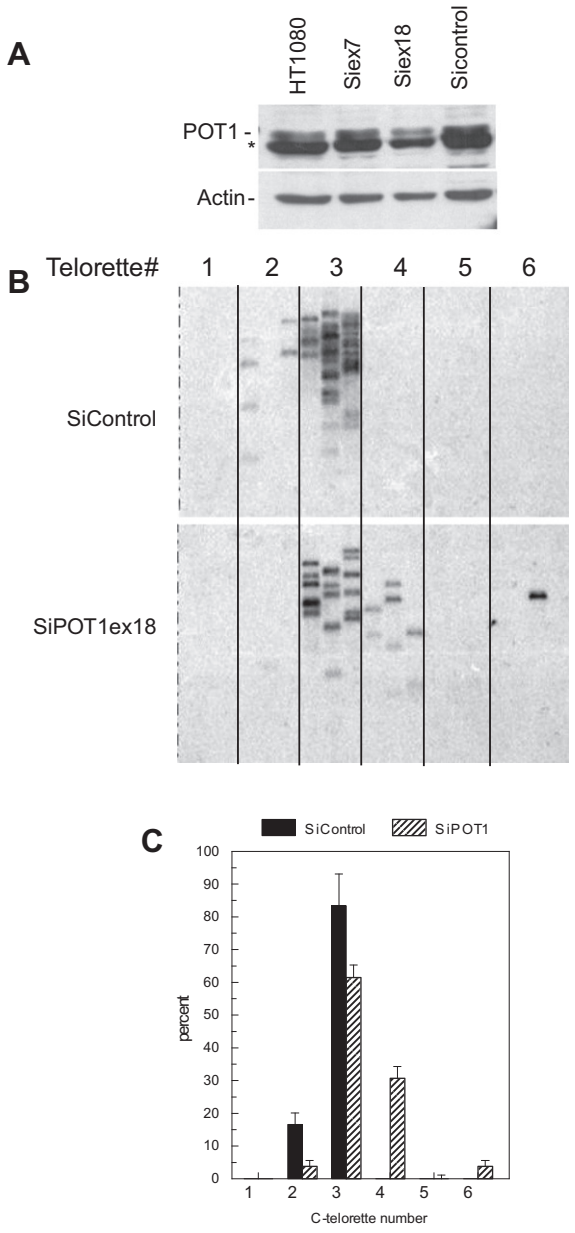

Fig. 8. Effect of POT1 depletion by siRNA on the terminal nucleotide composition at telomeric C-strand in HT1080 cells. (A) Western blot analysis of POT1 protein expression in HT1080 cells untreated or transfected with 100 nM siRNAs (siRNA control, siRNA POT1ex7, siRNA POT1ex18, as indicated) for 72 h. The asterisk indicated a non-specific band revealed by the POT1 antibody. β-actin was used as a control for protein loading. (B) C-STELA assay from HT1080 cells treated with siRNA control (100 nM) or siRNA POT1ex18 (100 nM), as indicated. C-telorette number (1–6) is indicated and each ligation was performed in triplicate. (C) Quantification of the experiment. In each lane, the telomere signal generated was quantified and expressed in percentage (mean ± SD, $n = 3$), with the total telomere signal generated by the six C-telorettes in each ligation defined as 100%.

samples in a study and subsequent ligations should be performed in parallel, as it was done for **360A**–**Br** or siRNA treatment. In these conditions, the assay in triplicate gives an acceptable reproducibility (compare HT1080 controls between days 4–12 and days 16–24 in Fig. 7C).

The only statistically significant variation in the C-telorette profile after 360A–Br treatment corresponded to a decrease of CCA-5′ and an increase of AAT-5′ ends, but without obvious change in the ATC-5′ predominance (see also Fig. S1 for quantifications at each passage where a trend for some significant variations is detectable). Similar results were obtained by measuring the number of telomere amplified instead of quantifying the radioactivity in each individual lane (Fig. S2). At first instance, these results suggest that **360A**–**Br** treatment does not induce the complete randomizing effect reported when POT1 is nearly completely depleted [10]. In our experimental conditions, we found that siRNA-mediated depletion of POT1 by 50% only triggers a partial but detectable randomization of the C-strand resection. Partial randomization was also found in HeLa cells partially depleted for POT1 (46%) using the same siRNA sequence [9]. Interestingly, these partial depletion of POT1 trigger the same relative variations in CAA-5′ and AAT-5′ ends than that observed after **360A**–**Br** treatment. We conclude that the effect of the ligand might correspond to a partial depletion of POT1.

A possible explanation for this limited action of the ligand may reside in the different mode of replication of telomeres between leading and lagging strand. Recent observations suggested that C-strand resection and G-overhang formation are uncoupled between leading and lagging strands at the end of telomere replication [7]. An additional step of C-strand fill-in by Polα recruited by the CST complex is necessary at lagging strand that requires the displacement of POT1 [7,53]. It is therefore possible that the recruitment of the nuclease responsible for the resection is directed by a fraction of POT1 interacting with TIN2–TRF1/2 that does not bind G-strand and not by the one interacting with G-strand. Since a G-quadruplex ligand is expected to block only the fraction of POT1 interacting with telomeric DNA, this might explain why a nearly complete depletion of POT1 would be necessary to observe the complete randomization of telomeric ends.

On the other hand, we also observed that the variation of C-strand 5′-ends induced by **360A**–**Br** is a transient event detectable between days 4–12 and not observed later. A decrease in the **360A**–**Br** growth inhibitory efficiency was also found between days 16–24 (see Fig. 5A), suggesting that the cell line may adapt to the treatment. In agreement, A549 cells induced to resistance to 360A presented increased expression of POT1 and TRF2 (C. Trentesaux, unpublished results).

Because of the minor modification induced by **360A**–**Br**, further works using additional cell lines models and/or different chemical series of G-quadruplex ligands are therefore needed to confirm these data.

Finally, since the C-STELA analysis only explore the behavior of XpYp telomere, it would be also interesting to address whether this situation could be generalized at other chromosome ends where STELA analysis is possible [54], or using the Universal STELA that bypass the need to design chromosome proximal primers in subtelomeric regions [55].

Acknowledgments

We thank Nathalie Rousselet and Aurore Guédin for technical assistance, Gregory Méchin for help in cell culture, Dr A. Londono-Vallejo and Dr L. Guittat for helpful discussions. This work was supported by a grant from the “ Ligue Nationale contre le Cancer, Equipe Labellisée 2010” to J.F. Riou and the Agence Nationale de la Recherche (ANR-09-BLAN-0355) to J.F. Riou and M.P. Teulade-Fichou. A. Sidibe was supported by a PhD fellowship from the “Ligue Nationale contre le Cancer”. E. Largy was supported by a joint fellowship from Centre National de la Recherche Scientifique (CNRS) and Institut Curie.

Appendix A. Supplementary data

Supplementary data related to this article can be found online at http://dx.doi.org/10.1016/j.biochi.2012.07.003.

References

[1] M.J. McEachern, A. Krauskopf, E.H. Blackburn, Telomeres and their control, Annu. Rev. Genet. 34 (2000) 331–358.
[2] T. de Lange, Shelterin: the protein complex that shapes and safeguards human telomeres, Genes Dev. 19 (2005) 2100–2110.
[3] R.E. Verdun, J. Karlseder, Replication and protection of telomeres, Nature 447 (2007) 924–931.
[4] A.J. Cesare, R.R. Reddel, Alternative lengthening of telomeres: models, mechanisms and implications, Nat. Rev. Genet. 11 (2010) 319–330.
[5] P. Martinez, M.A. Blasco, Telomeric and extra-telomeric roles for telomerase and the telomere-binding proteins, Nat. Rev. Cancer 11 (2011) 161–176.
[6] W. Palm, T. de Lange, How shelterin protects mammalian telomeres, Annu. Rev. Genet. 42 (2008) 301–334.
[7] S. Sampathi, W. Chai, Telomere replication: poised but puzzling, J. Cell. Mol. Med. 15 (2011) 3–13.
[8] A.J. Sfeir, W. Chai, J.W. Shay, W.E. Wright, Telomere-end processing the terminal nucleotides of human chromosomes, Mol. Cell. 18 (2005) 131–138.
[9] X. Dai, C. Huang, A. Bhusari, S. Sampathi, K. Schubert, W. Chai, Molecular steps of G-overhang generation at human telomeres and its function in chromosome end protection, EMBO J. 29 (2010) 2788–2801.
[10] D. Hockemeyer, A.J. Sfeir, J.W. Shay, W.E. Wright, T. de Lange, POT1 protects telomeres from a transient DNA damage response and determines how human chromosomes end, EMBO J. (2005).
[11] J.F. Sarthy, P. Baumann, Apollo-taking the lead in telomere protection, Mol. Cell. 39 (2010) 489–491.
[12] T.M. Bryan, P. Baumann, G-Quadruplexes: from guanine gels to chemotherapeutics, Mol. Biotechnol. (2011).
[13] A. De Cian, L. Lacroix, C. Douarre, N. Temime-Smaali, C. Trentesaux, J.F. Riou, J.L. Mergny, Targeting telomeres and telomerase, Biochimie 90 (2008) 131–155.
[14] D. Sen, W. Gilbert, Formation of parallel four-stranded complexes by guanine-rich motifs in DNA and its implications for meiosis, Nature 334 (1988) 364–366.
[15] A.T. Phan, Human telomeric G-quadruplex: structures of DNA and RNA sequences, FEBS J. 277 (2010) 1107–1117.
[16] S.M. Haider, S. Neidle, G.N. Parkinson, A structural analysis of G-quadruplex/ligand interactions, Biochimie 93 (2011) 1239–1251.
[17] H.J. Lipps, D. Rhodes, G-quadruplex structures: in vivo evidence and function, Trends Cell. Biol. 19 (2009) 414–422.
[18] J.L. Huppert, Structure, location and interactions of G-quadruplexes, FEBS J. 277 (2010) 3452–3458.
[19] S. Neidle, Human telomeric G-quadruplex: the current status of telomeric G-quadruplexes as therapeutic targets in human cancer, FEBS J. 277 (2010) 1118–1125.
[20] D. Monchaud, M.P. Teulade-Fichou, A hitchhiker's guide to G-quadruplex ligands, Org. Biomol. Chem. 6 (2008) 627–636.
[21] M. Folini, L. Venturini, G. Cimino-Reale, N. Zaffaroni, Telomeres as targets for anticancer therapies, Expert Opin. Ther. Targets 15 (2011) 579–593.
[22] E. Salvati, C. Leonetti, A. Rizzo, M. Scarsella, M. Mottolese, R. Galati, I. Sperduti, M.F. Stevens, M. D'Incalci, M. Blasco, G. Chiorino, S. Bauwens, B. Horard, E. Gilson, A. Stoppacciaro, G. Zupi, A. Biroccio, Telomere damage induced by the G-quadruplex ligand RHPS4 has an antitumor effect, J. Clin. Invest. 117 (2007) 3236–3247.
[23] H. Tahara, K. Shin-Ya, H. Seimiya, H. Yamada, T. Tsuruo, T. Ide, G-Quadruplex stabilization by telomestatin induces TRF2 protein dissociation from telomeres and anaphase bridge formation accompanied by loss of the 3′ telomeric overhang in cancer cells, Oncogene 25 (2006) 1955–1966.
[24] D. Gomez, R. Paterski, T. Lemarteleur, K. Shin-Ya, J.L. Mergny, J.F. Riou, Interaction of telomestatin with the telomeric single-strand overhang, J. Biol. Chem. 279 (2004) 41487–41494.
[25] D. Gomez, T. Wenner, B. Brassart, C. Douarre, M.F. O'Donohue, V. El Khoury, K. Shin-Ya, H. Morjani, C. Trentesaux, J.F. Riou, Telomestatin-induced telomere uncapping is modulated by POT1 through G-overhang extension in HT1080 human tumor cells, J. Biol. Chem. 281 (2006) 38721–38729.
[26] R. Rodriguez, S. Muller, J.A. Yeoman, C. Trentesaux, J.F. Riou, S. Balasubramanian, A novel small molecule that alters shelterin integrity and triggers a DNA-damage response at telomeres, J. Am. Chem. Soc. 130 (2008) 15758–15759.
[27] V. Casagrande, E. Salvati, A. Alvino, A. Bianco, A. Ciammaichella, C. D'Angelo, L. Ginnari-Satriani, A.M. Serrilli, S. Iachettini, C. Leonetti, S. Neidle, G. Ortaggi, M. Porru, A. Rizzo, M. Franceschin, A. Biroccio, N-cyclic bay-substituted perylene G-quadruplex ligands have selective antiproliferative effects on cancer cells and induce telomere damage, J. Med. Chem. 54 (2011) 1140–1156.
[28] D. Gomez, M.F. O'Donohue, T. Wenner, C. Douarre, J. Macadre, P. Koebel, M.J. Giraud-Panis, H. Kaplan, A. Kolkes, K. Shin-ya, J.F. Riou, The G-quadruplex ligand telomestatin inhibits POT1 binding to telomeric sequences in vitro and induces GFP-POT1 dissociation from telomeres in human cells, Cancer Res. 66 (2006) 6908–6912.
[29] B. Brassart, D. Gomez, A. De Cian, R. Paterski, A. Montagnac, K.H. Qui, N. Temime-Smaali, C. Trentesaux, J.L. Mergny, F. Gueritte, J.F. Riou, A new steroid derivative stabilizes g-quadruplexes and induces telomere uncapping in human tumor cells, Mol. Pharmacol. 72 (2007) 631–640.
[30] M. Gunaratnam, O. Greciano, C. Martins, A.P. Reszka, C.M. Schultes, H. Morjani, J.F. Riou, S. Neidle, Mechanism of acridine-based telomerase inhibition and telomere shortening, Biochem. Pharmacol. 74 (2007) 679–689.
[31] G. Pennarun, C. Granotier, L.R. Gauthier, D. Gomez, F. Hoffschir, E. Mandine, J.F. Riou, J.L. Mergny, P. Mailliet, F.D. Boussin, Apoptosis related to telomere instability and cell cycle alterations in human glioma cells treated by new highly selective G-quadruplex ligands, Oncogene 24 (2005) 2917–2928.
[32] M. Folini, C. Pivetta, G. Zagotto, C. De Marco, M. Palumbo, N. Zaffaroni, C. Sissi, Remarkable interference with telomeric function by a G-quadruplex selective bisantrene regioisomer, Biochem. Pharmacol. 79 (2010) 1781–1790.
[33] C. Granotier, G. Pennarun, L. Riou, F. Hoffschir, L.R. Gauthier, A. De Cian, D. Gomez, E. Mandine, J.F. Riou, J.L. Mergny, P. Mailliet, B. Dutrillaux, F.D. Boussin, Preferential binding of a G-quadruplex ligand to human chromosome ends, Nucleic Acids Res. 33 (2005) 4182–4190.
[34] R. Rodriguez, K.M. Miller, J.V. Forment, C.R. Bradshaw, M. Nikan, S. Britton, T. Oelschlaegel, B. Xhemalce, S. Balasubramanian, S.P. Jackson, Small-molecule-induced DNA damage identifies alternative DNA structures in human genes, Nat. Chem. Biol. 8 (2012) 301–310.
[35] T. Lemarteleur, D. Gomez, R. Paterski, E. Mandine, P. Mailliet, J.F. Riou, Stabilization of the c-myc gene promoter quadruplex by specific ligands' inhibitors of telomerase, Biochem. Biophys. Res. Commun. 323 (2004) 802–808.
[36] P.L. Tran, E. Largy, F. Hamon, M.P. Teulade-Fichou, J.L. Mergny, Fluorescence intercalator displacement assay for screening G4 ligands towards a variety of G-quadruplex structures, Biochimie 93 (2011) 1288–1296.
[37] R. Halder, J.F. Riou, M.P. Teulade-Fichou, T. Frickey, J.S. Hartig, Bisquinolinium compounds induce quadruplex-specific transcriptome changes in HeLa S3 cell lines, BMC Res. Notes 5 (2012) 138.
[38] M.Z. Hernandes, S.M. Cavalcanti, D.R. Moreira, W.F. de Azevedo Junior, A.C. Leite, Halogen atoms in the modern medicinal chemistry: hints for the drug design, Curr. Drug Targets 11 (2010) 303–314.
[39] E. Largy, F. Hamon, M.P. Teulade-Fichou, Development of a high-throughput G4-FID assay for screening and evaluation of small molecules binding quadruplex nucleic acid structures, Anal. Bioanal. Chem. (2011).
[40] H. Goulaouic, T. Roulon, O. Flamand, L. Grondard, F. Lavelle, J.F. Riou, Purification and characterization of human DNA topoisomerase IIIalpha, Nucleic Acids Res. 27 (1999) 2443–2450.
[41] D.M. Baird, J. Rowson, D. Wynford-Thomas, D. Kipling, Extensive allelic variation and ultrashort telomeres in senescent human cells, Nat. Genet. 33 (2003) 203–207.
[42] A. Picot, C. Feuvrie, C. Barsu, F. Malvolti, B. Le Guennic, H. Le Bozec, C. Andraud, L.c. Toupet, O. Maury, Synthesis, structures, optical properties, and TD-DFT studies of donor-Ï€-conjugated dipicolinic acid/ester/amide ligands, Tetrahedron 64 (2008) 399–411.
[43] N. Temime-Smaali, L. Guittat, A. Sidibe, K. Shin-ya, C. Trentesaux, J.F. Riou, The G-quadruplex ligand telomestatin impairs binding of topoisomerase IIIalpha to G-quadruplex-forming oligonucleotides and uncaps telomeres in ALT cells, PLoS One 4 (2009) e6919.
[44] S.M. Hampel, A. Sidibe, M. Gunaratnam, J.F. Riou, S. Neidle, Tetrasubstituted naphthalene diimide ligands with selectivity for telomeric G-quadruplexes and cancer cells, Bioorg. Med. Chem. Lett. 20 (2010) 6459–6463.
[45] L.R. Gauthier, C. Granotier, F. Hoffschir, O. Etienne, A. Ayouaz, C. Desmaze, P. Mailliet, D.S. Biard, F.D. Boussin, Rad51 and DNA-PKcs are involved in the generation of specific telomere aberrations induced by the quadruplex ligand 360A that impair mitotic cell progression and lead to cell death, Cell. Mol. Life Sci. (2011).
[46] C.M. Incles, C.M. Schultes, H. Kempski, H. Koehler, L.R. Kelland, S. Neidle, A G-quadruplex telomere targeting agent produces p16-associated senescence and chromosomal fusions in human prostate cancer cells, Mol. Cancer Ther. 3 (2004) 1201–1206.
[47] J.F. Riou, L. Guittat, P. Mailliet, A. Laoui, E. Renou, O. Petitgenet, F. Megnin-Chanet, C. Helene, J.L. Mergny, Cell senescence and telomere shortening induced by a new series of specific G-quadruplex DNA ligands, Proc. Natl. Acad. Sci. U. S. A. 99 (2002) 2672–2677.
[48] D.M. Baird, A.J. Jeffreys, N.J. Royle, Mechanisms underlying telomere repeat turnover, revealed by hypervariable variant repeat distribution patterns in the human Xp/Yp telomere, EMBO J. 14 (1995) 5433–5443.
[49] A. Renaud de la Faverie, F. Hamon, C. Di Primo, E. Largy, E. Dausse, L. Delauriere, C. Landras-Guetta, J.J. Toulme, M.P. Teulade-Fichou, J.L. Mergny, Nucleic acids targeted to drugs: SELEX against a quadruplex ligand, Biochimie 93 (2011) 1357–1367.
[50] G. Pennarun, F. Hoffschir, D. Revaud, C. Granotier, L.R. Gauthier, P. Mailliet, D.S. Biard, F.D. Boussin, ATR contributes to telomere maintenance in human cells, Nucleic Acids Res. 38 (2010) 2955–2963.
[51] T. Tauchi, K. Shin-Ya, G. Sashida, M. Sumi, A. Nakajima, T. Shimamoto, J.H. Ohyashiki, K. Ohyashiki, Activity of a novel G-quadruplex-interactive telomerase inhibitor, telomestatin (SOT-095), against human leukemia cells: involvement of ATM-dependent DNA damage response pathways, Oncogene 22 (2003) 5338–5347.
[52] S. Muller, D.A. Sander, M. Di Antonio, S. Matsis, J.F. Riou, R. Rodriguez, S. Balasubramanian, Pyridostatin analogues promote telomere dysfunction and long-term growth inhibition in human cancer cells, Org Biomol Chem, in press.
[53] M.J. Giraud-Panis, M.T. Teixeira, V. Geli, E. Gilson, CST meets shelterin to keep telomeres in check, Mol. Cell. 39 (2010) 665–676.
[54] B. Britt-Compton, J. Rowson, M. Locke, I. Mackenzie, D. Kipling, D.M. Baird, Structural stability and chromosome-specific telomere length is governed by cis-acting determinants in humans, Hum. Mol. Genet. 15 (2006) 725–733.
[55] L. Bendix, P.B. Horn, U.B. Jensen, I. Rubelj, S. Kolvraa, The load of short telomeres, estimated by a new method, universal STELA, correlates with number of senescent cells, Aging Cell 9 (2010) 383–397.